applied sciences

MDPI

Article

Radiomics Approach to the Detection of Prostate Cancer Using Multiparametric MRI: A Validation Study Using Prostate-Cancer-Tissue-Mimicking Phantoms

Faisal Alshomrani [1], Basim S. O. Alsaedi [2], Cheng Wei [1], Magdalena Szewczyk-Bieda [3], Stephen Gandy [3], Jennifer Wilson [3], Zhihong Huang [1] and Ghulam Nabi [4,*]

[1] School of Science and Engineering, University of Dundee, Dundee DD1 4HN, UK
[2] Department of Statistics, University of Tabuk, Tabuk 71491, Saudi Arabia
[3] Department of Clinical Radiology, Ninewells Hospital, Dundee DD1 9SY, UK
[4] Division of Imaging Sciences and Technology, School of Medicine, Ninewells Hospital, University of Dundee, Dundee DD1 9SY, UK
* Correspondence: g.nabi@dundee.ac.uk

Abstract: Over the last few years, a number of studies have quantified the role of radiomics, dynamic contrast enhancement and standard MRI (T2WI + DWI) in detecting prostate cancer; however, the aim of this paper was to assess the advantage of combining radiomics with other multiparametric magnetic resonance imaging (mpMRI) (T2-DWI-DCE) in improving the detection of prostate cancer. This study used 10 prostate-cancer-tissue-mimicking phantoms to obtain preclinical data. We then focused on 46 patients who underwent mpMRI and Transrectal Ultrasound (TRUS) guided biopsy between September 2016 and December 2017. The texture analysis parameters combined with the mpMRI and compared with the histopathology of TRUS biopsy have been assessed statistically by principal component analysis (PCA) and discriminant component analysis (DCA). The prediction model and goodness-of-fit were examined with the Akaike information criterion (AIC) and McFadden pseudo-R-squared. In the PCA, there was a higher separation between cancerous and noncancerous tissue in the preclinical compared with the clinical data. Both AIC and R2 showed an improvement in the model in cancer prediction by adding the radiomics to mpMRI. The discriminant analysis showed an accuracy of cancer prediction of 81% compared with 100% in the pre-clinical phantom data. Combining radiomics with mpMRI showed an improvement in prostate cancer prediction. The ex vivo experiments validated the findings of this study.

Keywords: mpMRI; prostate cancer; radiomic; dynamic contrast enhancement; tissue-mimicking phantom

Citation: Alshomrani, F.; Alsaedi, B.S.O.; Wei, C.; Szewczyk-Bieda, M.; Gandy, S.; Wilson, J.; Huang, Z.; Nabi, G. Radiomics Approach to the Detection of Prostate Cancer Using Multiparametric MRI: A Validation Study Using Prostate-Cancer-Tissue-Mimicking Phantoms. *Appl. Sci.* **2023**, *13*, 576. https://doi.org/10.3390/app13010576

Academic Editor: Qi-Huang Zheng

Received: 28 November 2022
Revised: 28 December 2022
Accepted: 29 December 2022
Published: 31 December 2022

1. Introduction

Prostate cancer is one of the most common cancers in men [1]. Diagnosing prostate cancer entails moving through the following steps: a digital rectal examination (DRE); estimation of prostate-specific antigen (PSA) in the blood; multiparametric MRI; and a biopsy under the guidance of ultrasound. Poor and imprecise detection of prostate cancer leads to morbidity and poor outcomes. Currently, 10 to 12 tissue samples (biopsies) are taken from the prostate to identify the grade of cancer. This approach may lead to haemorrhage and discomfort for the patients [2]; therefore, improving the sensitivity and specificity of prostate cancer diagnosis using imaging might change the current diagnostic protocol, such as by eliminating biopsy complications. Magnetic resonance imaging (MRI), in particular the use of multiparametric protocols in a pre-biopsy setting combined with targeted biopsies, has improved the detection rate of clinically significant prostate cancer [3].

Several imaging protocols (kinetic models) using parameters measuring changes in microcirculation have been described [4]. The diagnostic sensitivity rates achieved by combining quantitative measurements and semi-quantitative methods with mpMRI have

shown improvements in cancer detection [5]. The Prostate Imaging Reporting and Data System (PIRADS) was developed by the European Society of Urogenital Radiology (ESUR) to provide a standard protocol in the interpretation of the prostate images [6]; however, the PIRADS scoring system is subject to intra- and inter-operator variability [7]. Therefore, employing different quantification methods such as radiomics and dynamic contrast enhancement (DCE) extraction could potentially reduce the variability between observers.

Texture analyses and mathematical models to extract the image features have been reported to improve diagnostic accuracy [8]. These mathematical models provide a quantitative value, based on the grey level in the image, and can improve the detection of cancers [9]. Radiomics refers to a process of extracting large, quantifiable features from medical images which will transform the medical images to quantitative data [10]. In radiomics, an area of interest in defining the lesion and its pixel intensity will provide quantification data that represent a greyscale value in this area. A change in the pixel intensity of a particular area is strongly associated with a particular disease. In the histogram analysis, different parameters, such as the mean, standard deviation, mode, maximum, minimum, kurtosis and skewness, provide statistical information about the medical image [9]. The aims of this study were to assess the advantages of combining texture analysis parameters with other mpMRI (T2-DWI-DCE) parameters in improving the detection of prostate cancer. Moreover, the advantages of the of the combined approach were validated in pre-clinical study with tissue-mimicking phantom simulating the prostate cancer.

2. Materials and Methods

2.1. Study Population

This study had prior Caldicott institutional approval (Caldicott/IGTCAL6358). This study recruited 65 patients who were investigated for prostate cancer between 2016 and 2017 at Ninewells Hospital. The study focused on the group who had undergone both mpMRI and TRUS-guided biopsies. Patients with missing data for the DCE (n = 19) were excluded from the study. Each prostate was divided into 12 regions, totalling 780 regions for the cohort. Then, the analysis focused on 552 regions from 46 patients because in 19 patients, DCE data were missing. There were 40 regions with a Gleason score of 3 + 3, 88 regions had significant cancers (Gleason score 3 + 4 and more), and 424 regions were negative for cancer on biopsies. The study design is summarised in Figure 1.

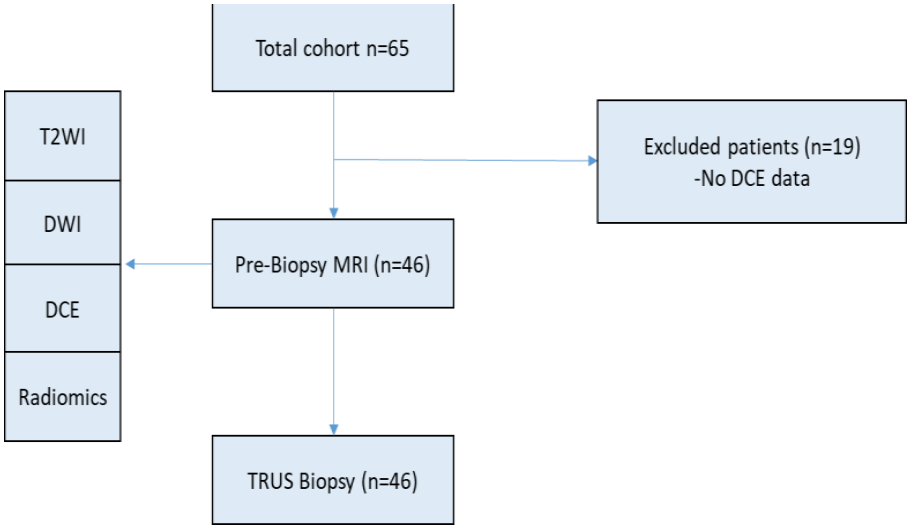

Figure 1. The study design in the clinical data and a prediction model were designed based on the combination of radiomics with mpMRI, and the findings were compared with the TRUS biopsy.

2.2. Tissue-Mimicking Material

In MRI, many different phantoms have been used; however, agar and agarose are the most commonly used [11]. The T2 relaxation time for agarose is similar to human tissue which is between 40 and 150 ms, therefore providing a good simulation to human tissue [12]. It is known that the cancer appearance in the peripheral zone will lead to reducing the signal intensity of the image; therefore, in the tissue-mimicking material, aluminium oxide (Al_2O_3) was used to change and obtain a different visualisation between cancerous and healthy tissue. In this study, different concentrations of agar were used, mainly 5% and 2% agar. The aim of using different concentrations was to mimic different tissues inside the prostate. The 2% agar was used to simulate the healthy tissue inside the prostate, whereas the agar 5% was used to simulate the cancerous tissue inside the prostate because the cancerous tissue will appear to have a higher stiffness inside the organ [13]. A mould was created using Solidwork 2018, 3D CAD, Dassault Systems, France with known dimensions ranging from 8 mm to 20 mm. Different percentages of contrast from aluminium oxide were used to distinguish between the two phantoms, which meant that 2% aluminium oxide was used for the smaller phantoms while 0.5% aluminium oxide was used for the bigger ones. Therefore, in each phantom, there were two regions, hyperintense-echoic and hypointense-echoic, as the cancer leads to the hypointense-echoic appearance in T2WI; the ROIs were drawn in the two regions to assess the ability of these parameters to distinguish between two areas.

2.3. MRI Protocol

MRI images were taken before the biopsy using a 3T scanner (Tim Trio, Siemens, Erlangen, Germany). The European Society of Uro-radiology protocol was applied for mpMRI to detect prostate cancer [14]. The MRI acquisition parameters are illustrated in Table 1. A body surface coil (Siemens, Erlangen, Germany) was used to obtain DCE images, and 2 mL/kg of Dotarem contrast agent was given to the patient intravenously. Before or during the scan, 1 mL of Buscopan was given to all patients to avoid movements in the bowel and rectum, which are located close to the prostate. Prostate gland imaging was carried out using different sequences (T1WI-T2WI-DWI and DCE). There was a short slice gap of 0.6 mm to avoid both the loss of useful information and missing any abnormality. In the DCE, there were very short TR and TE to acquire a series of images after the injection of the contrast. The slice thickness was 3 mm resolution to optimise the image resolution and the time scanning. The mpMRI images were analysed and scored by experienced uro-radiologists (with more than 5 years post-certification experience) using PIRADS v2.0.

Table 1. The MRI protocol during the scanning.

	T1WI	**High Resolution T2WI**			**DWI**		**DCE**
	Axial	**Sagittal**	**Axial**	**Coronal**	**DWI**	**DWI High *b*-Value**	**Dyn Gd-MRI**
Sequence	2DTSE	2DTSE	2DTSE	2DTSE	2DEPI	2DEPI	3D VIBE
TR (ms)	650	6000	4000	5000	3300	3300	4.76
TE (ms)	11	102	100	100	95	95	2.45
Flip angle (°)	150	140	150	150			10
Slice thickness (mm)	3	3	3	3	3	3	3
Slice gap (mm)	0.6	0.6	0.6	0.6	0	0	0.6
Resolution (pixels)	320	320	320	320	192	192	192
FOV (mm)	200	200	200	200	280	280	280
b-values (s/mm^2)					50, 100, 500, 1000	2000	
Temporal resolution (s)							4

2.4. Texture Analysis

Ten parameters were extracted in texture analysis exercise, including the mean and mode; most of these parameters have been reported to have a high association with

cancerous lesions [9]. The mean represented the average pixel intensity, while the standard deviation represented the dispersion of the histogram. The mode represented the value that mostly occurred within the region of interest. Skewness measured the asymmetry probability distribution of the histogram. In other words, if the result for skewness is close to 0, then the distribution of the information is symmetric, whereas an asymmetric distribution far from 0 is either positive skewness with more values having positive values or negative skewness with more values having negative values. Kurtosis measures the shape of the probability distribution, reflecting the shape of the curve, meaning that negative kurtosis indicated a flatter peak while positive kurtosis indicated a sharp peak. The parameters were extracted from T2WI, based on the histogram analysis first-order statistics. The radiomic features used in this study were mean, mode, median, range, variance, standard deviation, skewness, kurtosis, minimum and maximum. These parameters are summarised in Table S1. In this study, the prostate gland images were divided into 12 portions, based on the mapping biopsy report as shown in Figure S1. Subsequently, OLEA software (Olea Sphere®, v3; Olea Medical, La Ciotat, France) was used to perform the histogram analysis and extract quantified data from 12 regions from each prostate phantom as shown in Figure S2.

2.5. Dynamic Contrast Enhancement (DCE)

Dynamic contrast enhancement in MRI is based on a series of images taken by MRI before, during and after the injection of the contrast [15]. The most common contrast agent used in MRI is gadolinium. The contrast agent will shorten the T1 relaxation time, which will enhance the contrast in the organ; therefore, DCE is also known as permeability MRI. The acquisition time for collecting the image needs to be shortened by up to 5 s to analyse the early enhancement following injection of the contrast. The pharmacokinetic model was used to obtain a quantification about microvasculature permeability and there were some differences between the quantification results for different parameters due to the different models used in the different protocols [4]. The microvessels will form a network between the blood and tissue and, in most diseases that occur, certain changes occur in the microvessels; therefore, these changes could be used as a biomarker to detect a particular disease [4]. In this study, DCE was reported using 4D tissue software for the 12 portions of the prostate The Syngo Tissue 4D image post-processing platform (Siemens, Germany) as shown in Figure S3. The histopathology of the TRUS-guided biopsies was taken as a reference standard when evaluating the sensitivity and specificity of combining DCE from tissue 4D software, T2 weighted and DWI.

2.6. Statistical Analysis

Data processing was performed for both pre-clinical and clinical data, using SPSS 25 (IBM Corporation, New York, NY, US) and the free statistical software R (R Core Team, 2019). These tests were performed in 46 patients and for 10 phantom values. To estimate the area under the curve (AUC) for prediction, making use of multiple variables together with the existence of prostate cancer, receiver operating characteristic (ROC) curve analysis was conducted.

In this study, we adopted three multivariate approaches. PCA is one of the most commonly used statistical methodologies to investigate patterns in large, correlated datasets [16]. PCA explores the structures in the dataset and extracts principal components by mapping the original data to their equivalent components in the rotated space. It represents unsupervised modelling with no associated response, i.e., PCA will rotate and scale the image. PCA obtains a set of vectors (principal components) which are then used to measure the variability of the dataset, i.e., plotting the first and the second principal components will show the variation in the multidimensional dataset in a 2D plane. Discriminant analysis of principal component (DAPC) was conducted to identify and describe clusters without the influence of the response [17]. DAPC seeks to find differences between groups while minimising the variation within clusters. DAPC transforms the data first using PCA, which are then used to identify the existing clusters.

DCA was also considered to test the hypothesis of separation between the two groups, cancerous and healthy tissues [18]. DCA maximises the component axis for class separation. Unlike the previous methods, it is considered as supervised modelling. Thus, the response influences the components. Therefore, DCA is useful, not only as a support for PCA, but to also predict future samples.

In addition, univariate and multivariate logistic regression was used to assess the association of clinical characteristics and laboratory parameters to determine the best predictors of prostate cancer. The analysis started with all variables in the model, i.e., backward elimination. This allowed for the construction of the optimal regression equation to help determine the level of importance of each predictor variable. Two evaluation techniques were considered: AIC and McFadden's pseudo-R-squared. AIC estimates the likelihood of a model to predict future values (Akaike, 1974), which, in turn, can be used to evaluate a model [19]. A model with a lower AIC, among all other models, is considered to have a good fit. McFadden's pseudo-R-squared measures the goodness-of-fit of models. The test can range from 0 to 1, although it can never reach 1 because of its calculation. According to McFadden: "while R^2 index is a more familiar concept to planners who are experienced in ordinary regression analysis, it is not well-behaved a statistic as the R^2 measure, for maximum likelihood estimation. Those unfamiliar with R^2 should be forewarned that its values tend to be considerably lower than those of the R^2 index and should not be judged by the standards for a 'good fit' in ordinary regression analysis. For example, values of 0.2 to 0.4 for R^2 represent an excellent fit" [20].

Two-step logistic regression was performed to identify explanatory variables of significant prostate cancer. Mean, median, mode, standard deviation, sample variance minimum and maximum were individually entered into a univariate logistic regression model where the outcome was defined as having significant prostate cancer or not. Statistically significant variables were then entered into the multivariate logistic regression model. Odds ratio (OR), 95% confidence interval (95% CI) of odds ratio, and p values were recorded in Table S2.

The reproducibility of the radiomic measurements was assessed in a subgroup of 10 randomly selected phantoms by three observers. Excellent inter-rater reliability was shown with a correlation coefficient of 0.98 in a single measure ($p < 0.001$) in five radiomic parameters which were mean, median, mode, minimum, and maximum.

3. Results

3.1. Pre-Clinical

An ex vivo ROC curve was constructed to understand the effects of combining the radiomic parameters and the accuracy of each parameter. There was a high prediction of the cancerous lesions ex vivo, because the AUC was 1 after all radiomics in this study were combined as shown in Figure S4.

PCA was applied to generate a set of principal components to assess the difference between healthy and cancer patients. Based on Figure 2, non-cancerous materials were separated from cancer-mimicking materials in the first and second components. PCA was performed for the radiomic features in the phantoms to differentiate between cancerous and non-cancerous lesions. Figure 2 shows the score plot based on the first and second principal components. The first principal component explained 69% of the variation, and the second component explained 24% of the variation.

This result was unsurprising since they both explained 93.5% of the variation in the dataset. The distinction between non-cancerous and cancer-mimicking materials was explored with DAPC and DCA. The results, as shown in Figure 3 and Figure S5, illustrate the separation in support of the PCA.

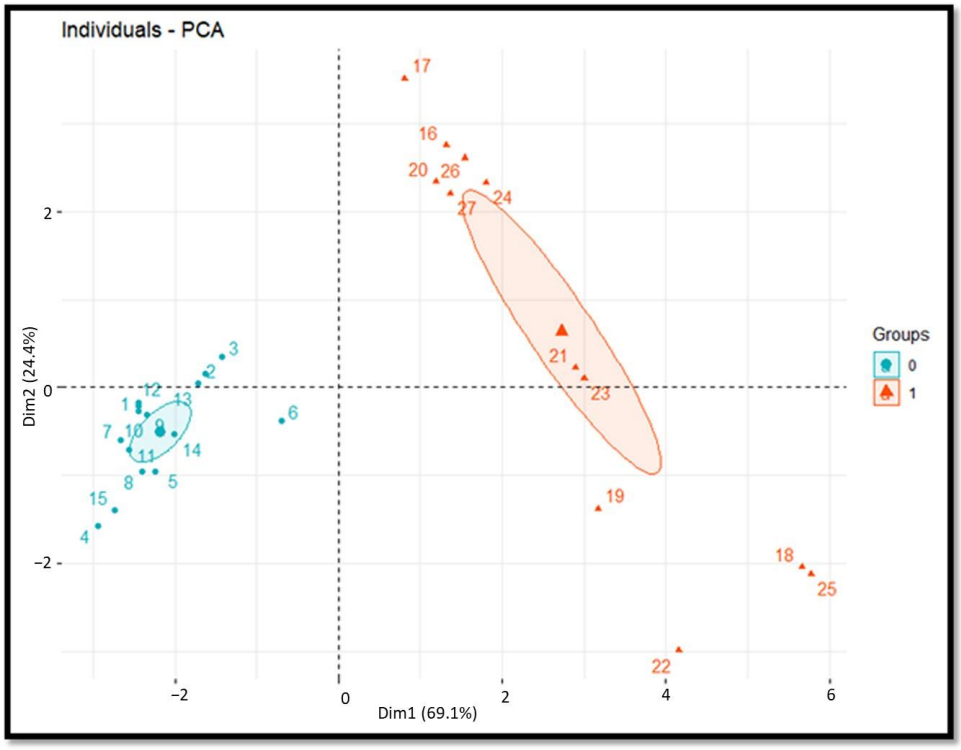

Figure 2. Score plot based on the first and second principal components. The first principal component explained 69% of the variation and the second component explained 24% of the variation. Group 0 represents normal regions in green, while group 1 represents cancerous regions in red. PCA was perfo¬rmed for the radiomic features in the phantoms to differentiate between cancerous and non-cancerous lesions. The simulation shows the score plot based on the first and second principal components.

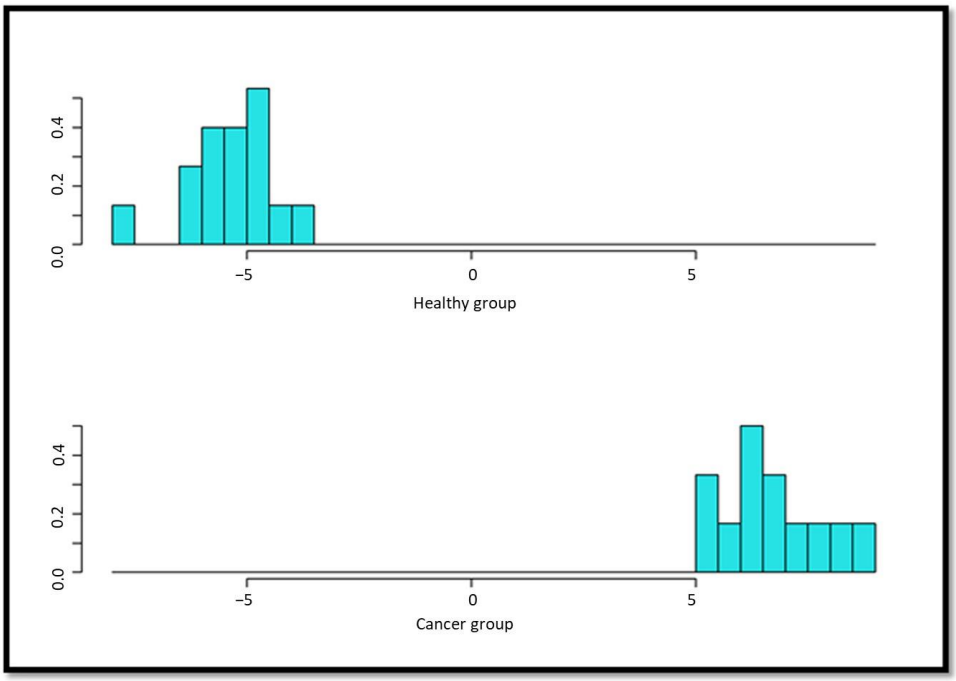

Figure 3. DCA and how it separates both groups with high accuracy and no overlap between the cancerous and healthy groups. The *x*-axis is the number of clusters, while the *y*-axis is the coefficient of discriminant analysis.

3.2. Clinical Data

Based on the ROC curve analysis of clinical data, there was a slight increase in the area under the curve of all texture analysis parameters combined with multiparametric MRI; the AUC was 0.82, whereas in the T2 + DWI alone, the AUC was 0.77. There was no significant difference between adding either DCE or texture analysis parameters to T2 + DWI; the AUC values were 0.79 and 0.82, respectively, as shown in Figure 4. For the clinically significant prostate cancer, the prediction model combining mpMRI and radiomics showed an improvement in AUC from 0.81 to 0.85.

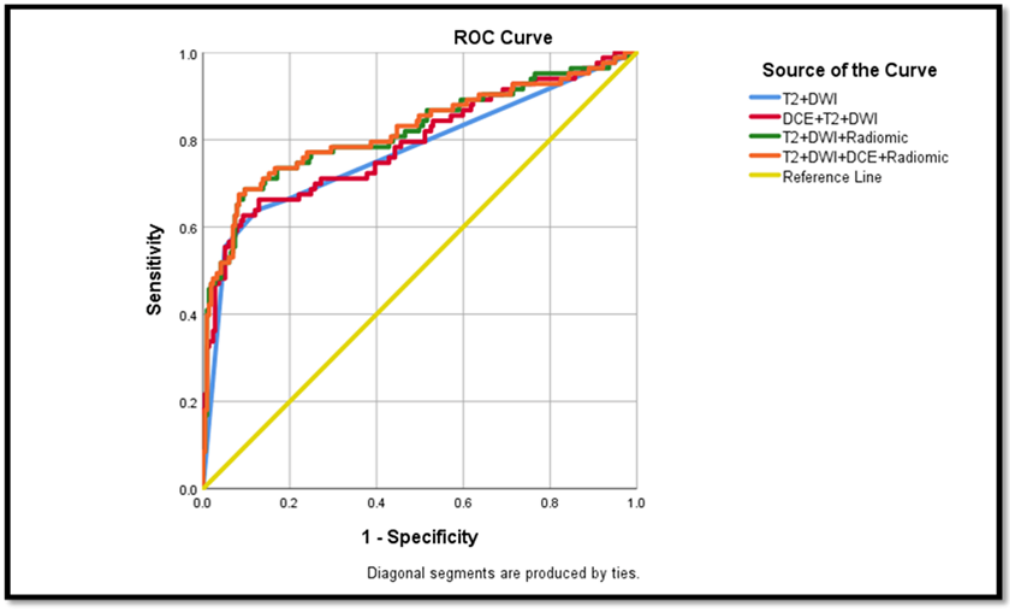

Figure 4. ROC curve for the clinical data. Four models were generated and compared with the gold standard TRUS biopsy. The orange curve is a combination between radiomics and mpMRI, showing a higher AUC of 0.82 compared with mpMRI alone in the red curve; the AUC was 0.77.

PCA was applied again to generate a set of principal components to assess the difference between healthy and cancerous tissues in the clinical data, using a combination of radiomics and DCE compared with the biopsy. The score plot, looking closely at the first two principal components, exhibited overlap between healthy tissue (normal prostate gland) and prostate cancer in some areas, which described the missed diagnosis and some separated areas indicating the efficiency of the adopted model in detecting the prostate cancer. Healthy tissue (normal prostate gland) was mostly separated from cancer patients, as shown in Figure 5.

Furthermore, the correlation matrix in Figure S6 showed a similar pattern of highly correlated variables, i.e., highly correlated variables may cause PCA to overemphasise their contribution.

DAPC was explored to identify clusters using PCA score vectors. The results were exemplified through the density plot of the two clusters, as shown in Figure 6.

The DAPC showed an almost clear separation between the two clusters. Finally, DCA showed a similar pattern to the previous methods, with a model accuracy of 81%, which was determined using training and testing data, as shown in Figure 7.

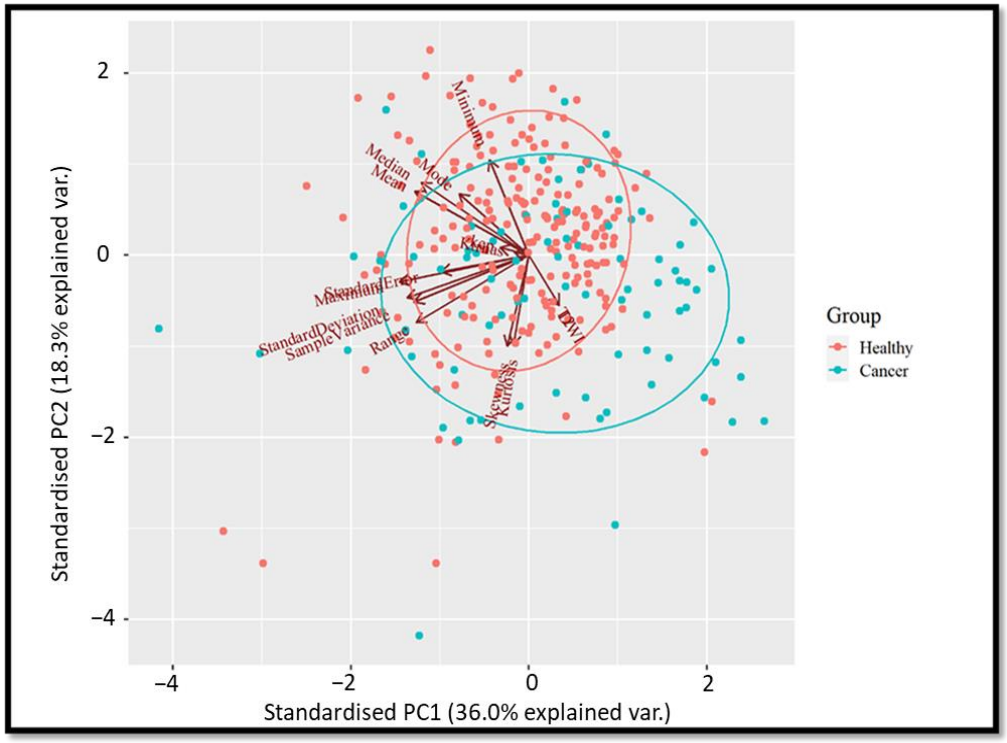

Figure 5. The score plot based on the first and second principal components. The first principal component explained 36% of the variation, and the second component analysis explained 18.3% of the variation. The prediction model was a combination of the radiomic features with mpMRI, and the findings were compared with the TRUS biopsy.

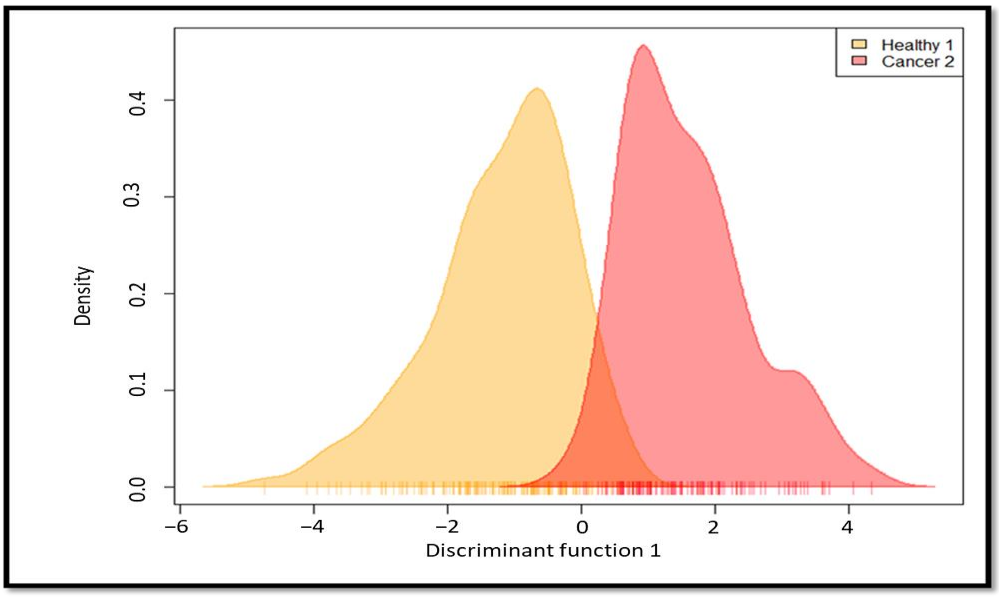

Figure 6. DAPC and how it clearly differentiates between the two groups healthy and cancerous tissue; there is a high degree of separation in most area. Red represents the cancerous tissues, whereas orange represents the non-cancerous tissues.

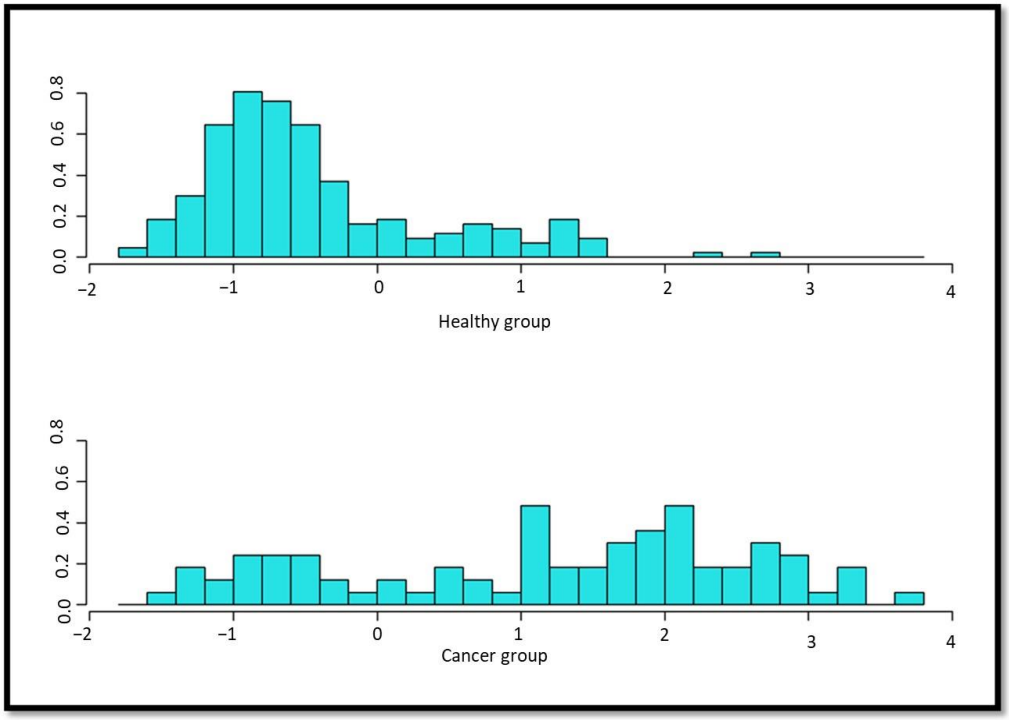

Figure 7. The DAPC and how it performed to separate both groups in the clinical data. Most patients in the healthy group accumulated a negative area, similar to the behaviour of the pre-clinical data. The *x*-axis is the number of clusters, while the *y*-axis is the coefficient of discriminant analysis.

3.3. Clinical Characteristics of Prostate Cancer

The overall model accuracy was evaluated using leave-one-out cross-validation (LOOCV). Based on 300 different samples (a resampling method were used to generate different samples), the model accuracy was 81.5% (CI 0.76, 0.85).

The data were modelled using backward selection via the logistic regression technique. This enabled evaluation of the multiple regression equation to determine the best predictors in the model. In Figure 8, both AIC and R2 McFadden of the logistic regression were given for a range of increased complexity. As the number of parameters increased, AIC started to decrease, and R2 McFadden started to increase. This showed that the model with all variables was a good fit for the data. T2WI was the first variable used in this model; then, DWI was added to it, followed by ktrans, and then kep, which are DCE parameters. Subsequently, the radiomics parameters were added to the model, which provided further improvements in the goodness-of-fit.

3.4. Correlation Analysis

In the correlation analysis, the minimum, median, mode and mean were significantly correlated with the Gleason score with p-value = 0.01, although other radiomic parameters did not significantly correlate with the Gleason score. The DCE parameters were not significantly correlated with the histopathology report: ktrans and kep were $p = 0.9$ and $p = 0.9$, respectively. After the prostates were divided into different zones, neither ktrans nor kep were significantly correlated with the histopathology report in PZ ($p = 0.86$ and $p = 0.93$, respectively); in TZ, ktrans was significantly correlated with the histopathology report ($p = 0.02$), whereas kep was not significantly correlated (p 0.5). In the PZ, four radiomic parameters (mean, median, mode and maximum) were significantly correlated with Gleason at $p < 0.05$, while in TZ, five radiomic parameters (mean, median, mode, maximum and SD) were significantly correlated with Gleason at $p < 0.05$. In the preclinical test, all radiomic parameters were significantly correlated with the gold standard (phantom tissue-mimicking material) with a p-value < 0.01.

Table S2 shows the outcomes of the logistic regression analysis and predictive variables of clinically significant cancer. On univariate analyses, mean, median, mode, SD, and SV were all significantly associated with clinically significant cancer ($p < 0.05$). The other radiomic features did not show any significance ($p > 0.05$), and were thus excluded from further analyses. In the multivariate analyses, modes were statistically significant and independently predictive of clinically significant cancer ($p = 0.04$).

There were 15% of significant cancers missed by the mpMRI which were reported by radiomics, and 8% of lesions missed by radiomics which were reported by mpMRI.

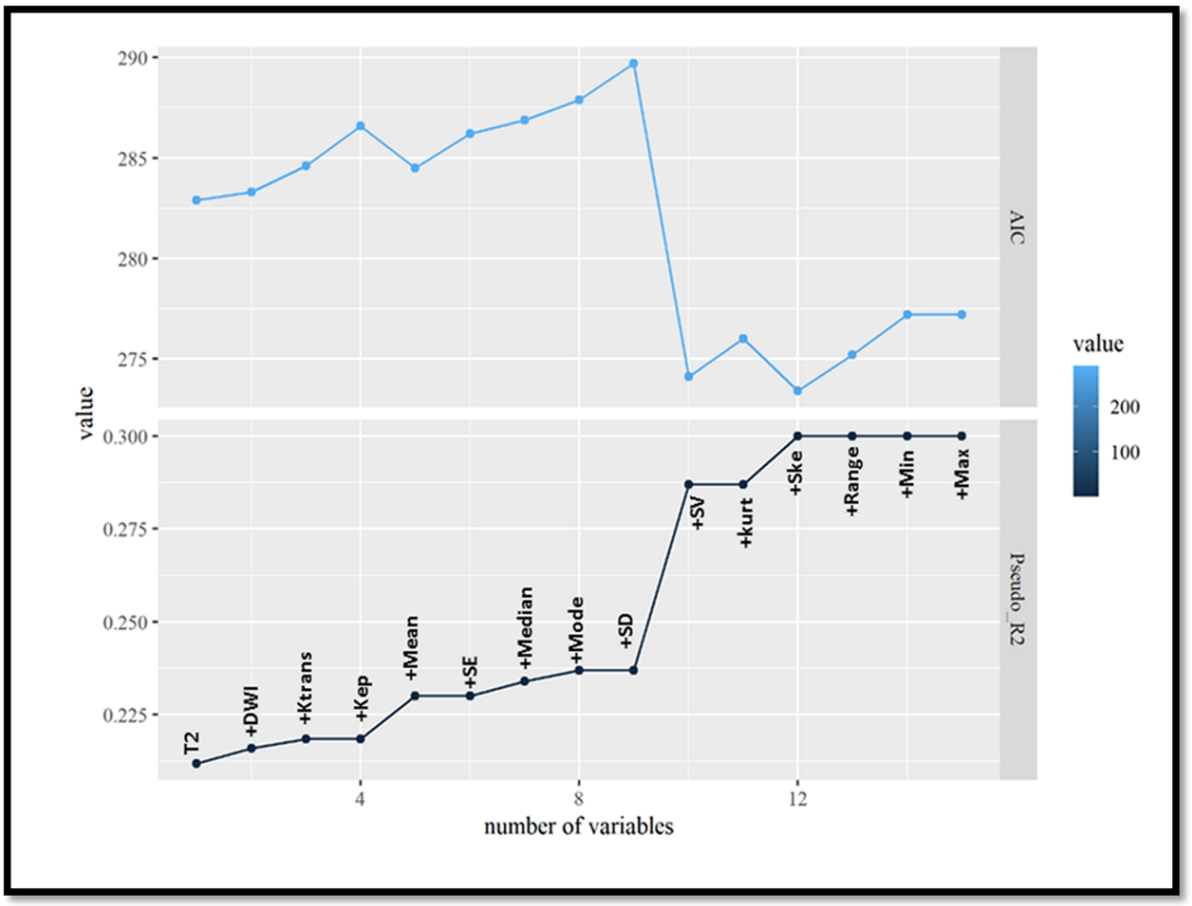

Figure 8. The AIC and Pseudo R2 (R2 McFadden) for multiple logistic regression equations. As the number of parameters increased, AIC started to decrease, and R2 McFadden started to increase.

4. Discussion

There is a clinical challenge in the reproducibility of PIRADS amongst radiologists and between different centres [21]. The quantification of features from images could be used as a marker of disease diagnosis, prognosis, and long-term outcomes. The texture analysis values in the detection of prostate cancer showed promising results [22]. The phantoms used in this study were a validation cohort to assess the combination between the radiomic features, providing an illustration of how the combination between the parameters differentiates between cancerous and non-cancerous images in clinical and pre-clinical practice. Combining multiparametric MRI findings with radiomics could potentially improve our understanding of disease and provided the necessary information needed for decision-making. There are reports that combining DCE features and T2WI increase AUC from 0.773 to 0.756 [23]. Excellent inter-rater reliability was shown with a correlation coefficient of 0.98 in a single measure ($p < 0.001$) in five radiomic parameters which were mean, median, mode minimum, and maximum and the same finding was found in other study as they have 0.9 correlation coefficients in the phantom [24]. A higher

reproducibility was suggested in a systematic review analysing the reproducibility of the radiomic parameters in different modalities (MRI, PET, and CT) and the analysis was performed in 481 studies supporting our findings [25]. We have shown that the combined approach improves the diagnostic accuracy of MRI and validates our findings through ex vivo phantom image analysis. The PCA showed a higher separation between non-cancerous and cancerous-mimicking materials in our pre-clinical validation study. This was confirmed in the clinical cohort where the combined approach performed well, albeit at lower rates. The homogenous phantom model in the preclinical setting presented higher diagnostic separation in contrast to clinical patient data as the signal intensity changed in the different prostate zones. Our results complement the findings of a previous study reporting a higher separation between the healthy and cancerous tissue. That study had a limited number of patients (n = 25) and only peripheral zones were analysed, in contrast to our study where the prostate glands were analysed for all 12 regions.

The combined approach of DCE and texture analysis with standard MRI (T2WI + DWI) improved the diagnostic accuracy; the AUC increased from 0.79 to 0.82. The discriminate analysis shows a high percentage of model accuracy in the separation group ex vivo and in vivo (100% and 81%, respectively), which is considered an acceptable proportion of separation of the healthy and cancerous tissue. Previously, reports have suggested that combining DCE and radiomics with standard MRI improves the detection rate of cancers in peripheral zones [26]; however, our model combining DCE, radiomics, and standard MRI increased the prediction of cancers in all zones.

This study showed that some radiomic features were significantly correlated with the histopathology, using the maximum, minimum, range, and mean; the same findings have been reported in previous studies [27], which support the addition of radiomic features into prediction models of prostate cancer. The DCE MRI appears to be controversial, because some studies suggest and highlight the importance of this parameter, whereas other studies have demonstrated limitations of this technique, especially in the temporal resolution of the sequence. The findings in this study were not significantly correlated with the histopathology reports [23]. Radiomic features are less invasive than DCE, and have a higher contribution in the prediction model of prostate cancer detection; therefore, they might replace the current methods of mpMRI which involve combinations between standard MRI (T2WI + DWI) and DCE; DCE contains a contrast agent administrated to the patients.

There were several limitations to this study. First, the study had a small number of patients. Second, the reference standard for comparison was systemic biopsies, which might have missed some lesions. Third, a mismatch may have occurred between the biopsy and region of interest seen in the mpMRI; however, we minimised this issue by applying the same protocol of the biopsy. Twelve regions were extracted from each MRI image.

5. Conclusions

This study showed that the first-order statistics extracted from radiomics, DCE and standard MRI (T2WI-DWI), could predict PCA results; pre-clinical experiments with tissue-mimicking phantoms validated the study findings. The contribution of radiomic features showed better results compared with DCE; therefore, it could replace it in the future and avoid the need for DCE being performed for the patient. This study showed that 15% of significant cancers which were missed by mpMRI were reported by radiomics, and 8% of lesions missed by radiomics were reported by mpMRI, indicating the importance of the combination of radiomics and mpMRI methods. The radiomic parameters showed an excellent inter-rater reliability, with a correlation coefficient of 0.98 in a single measure ($p < 0.001$) in five radiomic parameters. In this study, four radiomic features were significantly correlated with the histopathology.

Supplementary Materials: The following supporting information can be downloaded at: https://www.mdpi.com/article/10.3390/app13010576/s1, Figure S1: Extraction of the Radiomic feature by Olea software and this example shows 4 regions were extracted for the mid of the prostate and the drawing match with the TRUS protocol to compare the findings; Figure S2: Phantom which cancerous tissue simulation appeared with low signal intensity inside the red circle, and it is the similar appearance of cancer in the PZ in the T2WI of the prostate as it leads to reduce the signal intensity; Figure S3: The extracted DCE values from different areas inside the prostate of one patient using Tissue 4d software Table S1: MRI acquisition parameters; Figure S4: The ROC curve for the radiomic feature and the combined parameters between the 11 features has the highest AUC. 4 parameters reported a higher sensitivity and specificity compared with other parameters and these parameters were mean, median, mode, and minimum as their AUC were higher than 0.96; Figure S5: DAPC and how it separates both groups with high accuracy 100 % and no overlap between the cancerous and healthy which validates the use of the radiomic features in the clinical data; Figure S6: The correlation matrix between variables and the higher correlated variable can be excluded to give higher separation in PCA. The positive correlation between the variable was coloured with blue, while the negative correlation was coloured with red; Table S1: Shows the radiomic parameters used in this study; Table S2: Univariate and multivariate logistic regression analysis.

Author Contributions: Conceptualization, G.N. and Z.H.; methodology, F.A., B.S.O.A., C.W., S.G., M.S.-B., J.W., Z.H. and G.N.; investigation, F.A., B.S.O.A., C.W., S.G., J.W., M.S.-B., Z.H. and G.N.; writing—original draft, F.A. and G.N.; reviewing and editing, F.A., Z.H. and G.N.; funding acquisition, G.N.; supervision, G.N. and Z.H. All authors have read and agreed to the published version of the manuscript.

Funding: This research received no external funding.

Institutional Review Board Statement: This was a prospective, protocol-driven study with ethical approval obtained through the East of Scotland Ethical committee and Caldicott permission (IGTCAL6358)) to access healthcare follow-up data.

Informed Consent Statement: Informed consent was obtained from all subjects involved in the study.

Data Availability Statement: The data are available for scrutiny from external requests.

Conflicts of Interest: The authors declare no conflict of interest.

References

1. Yang, J.; Li, C.; Mudd, A.; Gu, X. LncRNA PVT1 Predicts Prognosis and Regulates Tumor Growth in Prostate Cancer. *Biosci. Biotechnol. Biochem.* **2017**, *81*, 1–6. [CrossRef] [PubMed]
2. Bloom, J.; Gurram, S.; Siddiqui, M.; Pinsky, P.; Parnes, H.; Linehan, W.M.; Merino, M.; Choyke, P.L.; Shih, J.H.; Turkbey, B.; et al. MRI-Targeted, Systematic, and Combined Biopsy for Prostate Cancer Diagnosis. *N. Engl. J. Med.* **2020**, *382*, 917–928. [CrossRef]
3. Rouvière, O.; Puech, P.; Renard-penna, R.; Claudon, M.; Roy, C.; Mège-lechevallier, F.; Decaussin-petrucci, M. Use of Prostate Systematic and Targeted Biopsy on the Basis of Multiparametric MRI in Biopsy-Naive Patients (MRI-FIRST): A Prospective, Multicentre, Paired Diagnostic Study. *Lancet Oncol.* **2019**, *20*, 100–109. [CrossRef]
4. Cuenod, C.A.; Balvay, D. Perfusion and Vascular Permeability: Basic Concepts and Measurement in DCE-CT and DCE-MRI. *Diagn. Interv. Imaging* **2013**, *94*, 1187–1204. [CrossRef] [PubMed]
5. Verma, S.; Turkbey, B.; Muradyan, N.; Rajesh, A.; Cornud, F.; Haider, M.A.; Choyke, P.L.; Harisinghani, M. Overview of Dynamic Contrast-Enhanced MRI in Prostate Cancer Diagnosis and Management. *Am. J. Roentgenol.* **2012**, *198*, 1277–1288. [CrossRef]
6. Score, G.; Song, W.; Bang, S.H.; Jeon, H.G.; Jeong, B.C.; Seo, S., II; Jeon, S.S.; Choi, H.Y.; Kim, C.K.; Lee, H.M. Role of PI-RADS Version 2 for Prediction of Upgrading in Biopsy-Proven Prostate Cancer With. *Clin. Genitourin. Cancer* **2018**, *16*, 281–287. [CrossRef]
7. Chung, A.G.; Member, S.; Shafiee, M.J.; Member, S.; Kumar, D. Discovery Radiomics for Multi-Parametric MRI Prostate Cancer Detection. *arXiv* **2015**, arXiv:1509.00111.
8. Wibmer, A.; Hricak, H.; Gondo, T.; Matsumoto, K.; Moskowitz, C.; Fine, S.W.; Reuter, V.E.; Eastham, J.; Sala, E.; Vargas, H.A. Haralick Texture Analysis of Prostate MRI: Utility for Differentiating Non-Cancerous Prostate from Prostate Cancer and Differentiating Prostate Cancers with Different Gleason Scores. *Eur. Radiol.* **2015**, *1*, 2840–2850. [CrossRef]
9. Just, N. Improving Tumour Heterogeneity MRI Assessment with Histograms. *Br. J. Cancer* **2014**, *111*, 2205–2213. [CrossRef]
10. Incoronato, M.; Aiello, M.; Infante, T.; Cavaliere, C.; Grimaldi, A.M.; Mirabelli, P.; Monti, S.; Salvatore, M. Radiogenomic Analysis of Oncological Data: A Technical Survey. *Int. J. Mol. Sci.* **2017**, *18*, 805. [CrossRef]
11. Hellerbach, A.; Schuster, V.; Jansen, A.; Sommer, J. MRI Phantoms—Are There Alternatives to Agar? *PLoS ONE* **2013**, *8*, e70343. [CrossRef] [PubMed]

12. Wyatt, C.R.; Smith, T.B.; Rooney, W.D.; Guimaraes, A.R. Multi—Parametric T 2 * Magnetic Resonance Fingerprinting Using Variable Echo Times. *NMR Biomed.* **2018**, *31*, e3951. [CrossRef] [PubMed]
13. Cao, R.; Huang, Z.; Varghese, T.; Nabi, G. Tissue Mimicking Materials for the Detection of Prostate Cancer Using Shear Wave Elastography: A Validation Study. *Med. Phys.* **2013**, *40*, 22903. [CrossRef] [PubMed]
14. Padhani, A.R.; Weinreb, J.; Rosenkrantz, A.B.; Villeirs, G.; Turkbey, B.; Barentsz, J.; Catto, J. Prostate Imaging-Reporting and Data System Steering Committee: PI-RADS v2 Status Update and Future Directions. *Eur. Urol.* **2018**, *75*, 385–396. [CrossRef] [PubMed]
15. Connor, J.P.B.O.; Tofts, P.S.; Miles, K.A.; Thompson, G.; Jackson, A. Dynamic Contrast-Enhanced Imaging Techniques: CT and MRI. *Br. J. Radiol.* **2011**, *84*, S112–S120. [CrossRef]
16. Williams, L.J. Principal Component Analysis. *Wiley Interdiscip. Rev. Comput. Stat.* **2010**, *2*, 433–459. [CrossRef]
17. Jombart, T.; Devillard, S.; Balloux, F. Discriminant Analysis of Principal Components: A New Method for the Analysis of Genetically Structured Populations. *BMC Genet.* **2010**, *11*, 94. [CrossRef]
18. Abdi, L.; Ghodsi, A. Discriminant Component Analysis via Distance Correlation Maximization. *Pattern Recognit.* **2020**, *98*, 107052. [CrossRef]
19. Aike, H.A.I. A New Look at the Statistical Model Identification. *IEEE Trans. Autom. Control.* **1974**, *19*, 716–723. [CrossRef]
20. McFadden, D. *R2.Pdf*, 474th ed.; Yale University: New Haven, CO, USA, 1977.
21. Coil, E.P.; Baldisserotto, M.; Neto, E.J.D.; Carvalhal, G.; De Toledo, A.F.; De Almeida, C.M.; Cairoli, C.E.D.; Silva, D.D.O.; Carvalhal, E.; Paganin, R.P.; et al. Validation of PI-RADS v. 2 for Prostate Cancer Diagnosis with MRI at 3T Using. *J. Magn. Reson. Imaging* **2016**, *44*, 1354–1359. [CrossRef]
22. Pi-rads, R.M.; Yang, S.; Wei, C.; Wu, J.; Li, X.; Zhao, W. Prostate Cancer Differentiation and Aggressiveness: Assessment with a Radiomic-Based Model vs. PI-RADS v2. *J. Magn. Reson. Imaging.* **2019**, *49*, 875–884. [CrossRef]
23. Berman, R.M.; Brown, A.M.; Chang, S.D.; Sankineni, S.; Kadakia, M.; Wood, B.J.; Pinto, P.A.; Choyke, P.L.; Turkbey, B. DCE MRI of Prostate Cancer. *Abdom. Radiol.* **2016**, *41*, 844–853. [CrossRef] [PubMed]
24. Bologna, M.; Corino, V.D.A.; Mainardi, L.T. Assessment of the Effect of Intensity Standardization on the Reliability of T1-Weighted MRI Radiomic Features: Experiment on a Virtual Phantom. In Proceedings of the 2019 41st Annual International Conference of the IEEE Engineering in Medicine and Biology Society (EMBC), Berlin, Germany, 23–27 July 2019; IEEE: Piscataway, NJ, USA, 2019; pp. 413–416.
25. Xue, C.; Yuan, J.; Lo, G.G.; Chang, A.T.Y.; Poon, D.M.C.; Wong, O.L.; Zhou, Y.; Chu, W.C.W. Radiomics Feature Reliability Assessed by Intraclass Correlation Coefficient: A Systematic Review. *Quant. Imaging Med. Surg.* **2021**, *11*, 4431. [CrossRef] [PubMed]
26. Kuess, P.; Andrzejewski, P.; Nilsson, D.; Georg, P.; Knoth, J.; Susani, M.; Trygg, J.; Helbich, T.H.; Polanec, S.H.; Georg, D.; et al. Association between Pathology and Texture Features of Multi Parametric MRI of the Prostate Association between Pathology and Texture Features of Multi Parametric MRI of the Prostate. *Phys. Med. Biol.* **2017**, *62*, 7833. [CrossRef] [PubMed]
27. Liu, B.; Cheng, J.; Guo, D.J.; He, X.J.; Luo, Y.D.; Zeng, Y.; Li, C.M. Prediction of Prostate Cancer Aggressiveness with a Combination of Radiomics and Machine Learning-Based Analysis of Dynamic Contrast-Enhanced MRI. *Clin. Radiol.* **2019**, *74*, 896-e1. [CrossRef] [PubMed]